Aperture Tolerances for Neutron-Imaging Systems in Inertial Confinement Fusion

Introduction

The inertial confinement fusion (ICF) approach to fusion ignition relies on inertia to compress the fuel to ignition conditions. A major goal of ICF research is the generation of net energy by imploding targets containing deuterium–tritium (DT) fuel, using lasers, x rays generated by lasers, pulsed power, or ion beams.[1] To achieve ignition, it is necessary for the target irradiation to be as symmetric as possible, minimizing hydrodynamic instabilities that reduce the implosion efficiency. To validate simulations of the implosions, one must measure or infer the density and temperature distribution of the fuel at peak compression.[2] This requires a number of target diagnostics that typically utilize x rays and fusion-reaction products emitted from the core.[3–5]

For example, an x-ray image of an ICF core provides information about the spatial structure of several complex processes within the target that are directly related to the fusion reactions. The x-ray image depends on the spatial and temporal profiles of plasma density and electron temperature. Diagnostics based on neutron emission provide a direct measure of the fusion burn region. These diagnostics are used to infer the fuel areal density, neutron yield, fuel ion temperature, and bang time.[2] The spatial distribution of the burning fuel can be directly determined by imaging the primary and scattered neutron emission from the core[6] (in this context, primary neutron images are based on the thermally broadened 14-MeV neutron emission from D-T fusion reactions in the core, while scattered neutron images are based on primary neutrons that scatter from the dense fuel to energies well below the 14-MeV line emission; these neutrons provide an image of the cold-fuel distribution in a non-igniting implosion). A neutron image is obtained by placing an appropriate aperture in front of a spatially sensitive neutron detector. These apertures typically code the spatial distribution from the source by differentially attenuating the neutron flux. The reconstruction of the core image requires precise knowledge of the aperture geometry.[7] Neutron imaging would be used to identify ignition-failure mechanisms such as poor implosion symmetry or inadequate convergence/areal density. Neutron imaging is used on the OMEGA[7] laser to measure the core symmetry of gas-filled plastic shells and energy-scaled, ignition-relevant cryogenic target implosions.[8]

A spatially sensitive neutron detector can be based on an array of scintillators or on a bubble chamber.[9] For a required image resolution, the system design considerations include magnification, the signal-to-noise (S/N) ratio, aperture-alignment accuracy, aperture-fabrication tolerances, neutron energy, neutron yield, field of view, and the detector spatial resolution. Here the S/N ratio refers to unwanted neutron signals from scattering sites near the imaging line of sight. This noise typically scales with the signal (primary yield) and can be reduced by shielding the detector. The impact of this noise can be further reduced by acquiring a flat-field (i.e., no aperture) image in a high-field implosion. For the work presented here, no attempt was made to include a neutron noise component in the simulations. For ICF experiments on laser facilities such as OMEGA[7] and the National Ignition Facility (NIF),[10] optimization of the system design is a complex process and understanding the effects and trade-offs of component tolerances requires simulations and image analysis. This article will discuss system design considerations and will focus on the resolution limitations introduced by the aperture alignment and fabrication tolerances.

Design Considerations for Neutron Imaging for ICF

Neutron-imaging (NI) systems use extended pinholes or penumbral apertures (with annular apertures as a particular case of the second) to generate images on the detector plane.[6] A full system consists of a neutron source, an aperture, an alignment system, and a neutron-sensitive detector (Fig. 112.1). When the neutrons pass from the source through the aperture, their spatial intensity at the detector plane is modulated according to the shape of the aperture. The alignment and type of aperture define the image size, shape, and resolution on the detector plane. The aperture's three-dimensional shape is described by a two-variable point-spread function (PSF). The magnification M of the system is the ratio of source–detector distance L divided by the source-aperture distance ℓ.

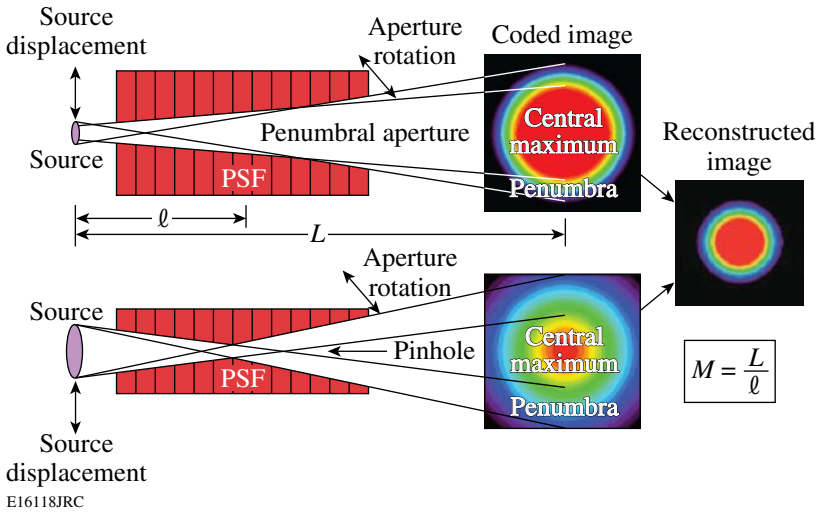

Figure 112.1
Schematic diagrams of penumbral and pinhole-imaging devices. The functional information for source-image reconstruction comes from the penumbral area of the image on the detector plane (except for the case when the pinhole is much smaller than the source). The magnification of the system M is the ratio of the source–detector distance L divided by the source-aperture distance ℓ.

1. Pinhole Imaging

Neutron-based pinhole imaging works on the same principle as an optical pinhole camera, with the source image directly displayed on the detector. Additional processing is required for a pinhole diameter comparable to or larger than the desired resolution. Due to the finite neutron range inside the materials, the pinhole is extended radially and not limited to a single plane along the observation axis. The image on the detector plane consists of a central maximum surrounded by a large penumbra. The small diameter (typically of the order of 10 μm) of the aperture makes it difficult to fabricate the aperture with the required precision and constitutes one of the main sources of error in the measured/reconstructed image. Relative to a thin aperture (e.g., an optical pinhole), it is more difficult to obtain a clear image due to the finite depth of focus of a neutron aperture (a neutron aperture simply attenuates the neutron flux rather than blocking it from reaching the detector). The image may directly represent the source, as it does for an optical pinhole camera, but it is formed from only those neutrons passing through a small aperture, limiting the resolution and S/N ratio for low-yield (for example, $\leq 10^{14}$) implosions.[11]

2. Penumbral Imaging

Penumbral imaging with an aperture larger than the source size is a coded-aperture-imaging technique (i.e., the image seen on the detector's plane is not the exact representation of the source but is defined by the PSF of the aperture).[5] With a penumbral aperture, the image consists of a uniform, bright central region surrounded by a partially illuminated penumbra. The source image is encoded in the penumbra of the detected image (the bright central region receives signals from the entire source area and does not provide spatial information). The diameter of a penumbral aperture is typically larger than the source and, therefore, for a comparable resolution, should be easier to fabricate, characterize, and align than a pinhole. Due to the larger solid angle, the image is formed from many more neutrons than for a pinhole; therefore, for a given yield, it typically has an intrinsically higher S/N ratio.[12]

The coded image must be deconvolved to produce an image of the neutron source. This process requires precise knowledge of the aperture point-spread function and the flat-field response of the imaging detector.[6] Therefore, a penumbral aperture is designed to be as isoplanatic as possible. This means that the aperture PSF is independent of the source point in the field of view. In practice, this is difficult to do and is the primary reason for the study of alignment sensitivity.

For both types of apertures, uncertainties in the exact shape (due to finite fabrication tolerances) lead to errors in the reconstructed image due to uncertainties in the calculated PSF. For brighter neutron sources (neutrons per source element), the S/N ratio improves faster for pinholes than for penumbral apertures, making pinholes the preferred aperture type of very high yield (for example, $\geq 10^{16}$) ICF imaging.[10]

Reconstruction of the Detector-Plane Image

Nyquist's theorem states that in order to accurately reconstruct a signal based on periodic sampling, the sampling frequency must be at least twice the maximum frequency of the signal. This limits the maximum resolution of a pixelated imaging system to $2\delta(\text{pixel})/M$, where M is the magnification of the system and $\delta(\text{pixel})$ represents the pixel resolution on the image plane.[13] To diminish the effect of image aliasing (i.e., pixelation of image), various anti-aliasing techniques can be

applied. The numerical noise in the signal (in this case the noise is associated with the image reconstruction) is typically given by Poisson statistics, and its reduction requires low-bandpass filtration; i.e., the signal has a frequency higher than a conveniently chosen cutoff value.[14]

In the neutron-detection measurements associated with imaging, random errors arise from various sources, such as misalignment, detector noise, etc. In most of the cases, a Gaussian distribution, or other similar type, can be used to characterize the random errors encountered. The standard deviation of the distribution is used as a measure of the uncertainty. For a neutron image, the relevant sources of error are due to the detector noise (typically associated with flat-field statistics), aperture alignment, pixel resolution of the detector, and the recoil distances of the nuclei in the detector. Therefore, the overall measurement uncertainty is given by[14]

$$\sigma_s = \sqrt{\sigma_{\text{noise}}^2 + \sigma_{\text{align}}^2 + \sigma_{\text{pixel}}^2 + \sigma_{\text{rec}}^2}\,, \tag{1}$$

where the indices *noise*, *align*, *pixel*, and *rec* represent the errors induced by noise, alignment, pixel, and recoil distance. The resolution of the system (i.e., the scale of the smallest resolvable point in the source under ideal conditions) can be written based on similar assumptions. Because the error given by Poisson statistics is inversely proportional to the cutoff frequency k_c (at which point the noise starts to dominate), the resolution of the imaging system can be written as[14]

$$\delta_s = \sqrt{\frac{1}{k_c^2} + \delta_{\text{align}}^2 + \left(\frac{2\delta_{\text{pixel}}}{M}\right)^2 + \left(\frac{\delta_{\text{rec}}}{M}\right)}\,, \tag{2}$$

where M is the magnification of the system and δ_{align}, δ_{pixel}, and δ_{rec} are the resolution components given by alignment error, the finite pixelation of the detector, and the particle recoil distance from the interaction of the neutrons with the detector medium. A neutron-imaging system could, in principle, achieve an improved resolution by using a high magnification, but a higher value for M increases the sensitivity to alignment errors. Keeping the other parameters fixed, a large target–aperture distance provides a better resolution as M increases in Eq. (2). Higher neutron yields increase the value of k_c in Eq. (2) and decrease the resolution limit of the instrument.

A coded penumbral image and, in most cases, a coded pinhole image on the detector plane can be deconvolved using an inverse Fourier transform.[5] By considering the magnified image of the source without any penumbral blurring as a function of coordinates $f(x,y)$ and the image created by a point source (or the PSF) as $g(x,y)$, an image on the detector plane $h(x,y)$ is created through the convolution of the first two functions:

$$\begin{aligned} h(x,y) &= f(x,y) \circ g(x,y) \\ &= \iint f(x',y')\,g(x-x',y-y')\,dx'\,dy'. \end{aligned} \tag{3}$$

A deconvolution of the source image can be obtained by using the convolution theorem of the Fourier transform. Since $H(k,l) = \mathrm{F}(k,l)\,G(k,l)$, with H, F, G the Fourier transforms of h, f, g,

$$\mathrm{F}(k,l) = \frac{H(k,l)}{G(k,l)}\,, \tag{4}$$

and the source image becomes

$$f(x,y) = \mathrm{F}^{-1}\left[\frac{H(k,l)}{G(k,l)}\right] = \mathrm{F}^{-1}\left\{\frac{\mathrm{F}\left[h(x,y)\right]}{\mathrm{F}\left[g(x,y)\right]}\right\}, \tag{5}$$

where F and F^{-1} are the Fourier and inverse Fourier transforms. A Wiener filter[12] can be used to reduce the noise levels by replacing

$$G(k,l) = \mathrm{F}\left[g(x,y)\right] = \frac{\left|H(k,l)\right|}{\left|H(k,l)\right|^2 + \gamma}\,, \tag{6}$$

where γ is an arbitrary correction factor (always positive) chosen to minimize the noise on the reconstructed image.

Neutron-Imaging Design Tool

To investigate the influences of various parameters of a NI system on the quality of the reconstructed image, a design tool has been developed. The code was written in PV Wave [http://www.vni.com], and Eqs. (5) and (6) have been used to reconstruct the encoded image. The source and detector plane are described by arrays that define the maximum theoretical system resolution. Various source distributions and intensity profiles can be generated. Noise can be added to simulate neutron background, but for the work presented here no neutron-related noise was added (any such noise can be subtracted from the image recorded on the detector plane). The aperture is described as a succession of thin layers with fixed openings along the particle-flux direction, and the resulting image on the detector plane is created by summing the neutron attenuations of the individual layers. A PSF for the aperture is generated by

ray tracing between the array elements of source and detector. The rays are treated as optical, to precisely define the thin-layered edges of each aperture. In this way, a variety of apertures can be simulated (pinholes and penumbral, cylindrical, biconic, or annular). The only limitation for the simulations is the available computational power. Fabrication and alignment tolerances can be determined by direct simulation using realistic source distributions and detector responses.

The simulations consist of defining a source distribution (shape and brightness) using an array of small source elements (the pixel size in the source is smaller than the system resolution) and calculating the PSF using ray tracing between the source elements and the detector elements (pixels). The pixelation of the detector is typical for existing neutron-imaging systems. The shapes of the reconstructed images can then be compared with the original source to determine if features associated with the aperture shape and alignment would be measurable in an actual imaging system.

For any NI system, several factors determine the characteristics of the image on the detector plane and those of the reconstructed image: The magnification determines the size of the image on the detector plane. If a large magnification is achieved by increasing the source-to-detector distance, a larger detector for a given source size or field of view is required. The aperture regulates the neutron flux on the detector. Its size determines, as much as the magnification, the dimension of the image on the detector plane for penumbral imaging systems. The aperture thickness and material determine its leakage to neutrons, and its shape controls the characteristics of the coded image and, therefore, the accuracy of the deconvolution process. The aperture is also sensitive to misalignment and can also be simulated. Another factor is the sensitivity of the recording medium. Apart from any intrinsic pixel resolution imposed by the detector dimensions, the detector resolution is ultimately limited by the recoil length of the elastically scattered nuclei at the detector material (e.g., protons in a CH-based scintillator). The last two factors to be taken into consideration are the neutron-scattering sources near the imaging line of sight and the field of view (limits resolution via the PSF).

Specific Examples

This design tool has been tested against simple cases having analytical solutions. Good agreement between the analytic calculations and numerical simulations suggests that the technique can be applied to complex aperture assemblies. For a point source, a perfect fit was obtained between the reconstructed and the analytically calculated images. For a circular flat source (constant brightness), the relative difference between the reconstructed and the analytically calculated images was in the range of 1% (due to the fact that the circular source was approximated by an array and its element centers were either outside or inside the source radius, changing the calculated values of the inverse Fourier transform), as shown in Fig. 112.2.

Data images from implosions generated by OMEGA shots were reconstructed using the technique described above [Fig. 112.3(a)] and compared with the results obtained by using the method described in Ref. 14 (filtered autocorrelation) and shown in Fig. 112.3(b). The biconic aperture used had a 200-μm field of view (FOV), a thickness of 100 mm, and a central diameter of 2 mm. The measured diameter of the neutron source size was ~50 μm, the source–aperture distance was 26 cm, and the source–detector distance was 800 cm, yielding a magnification of 30.8. The DT neutron yield was 8.5×10^{12}.

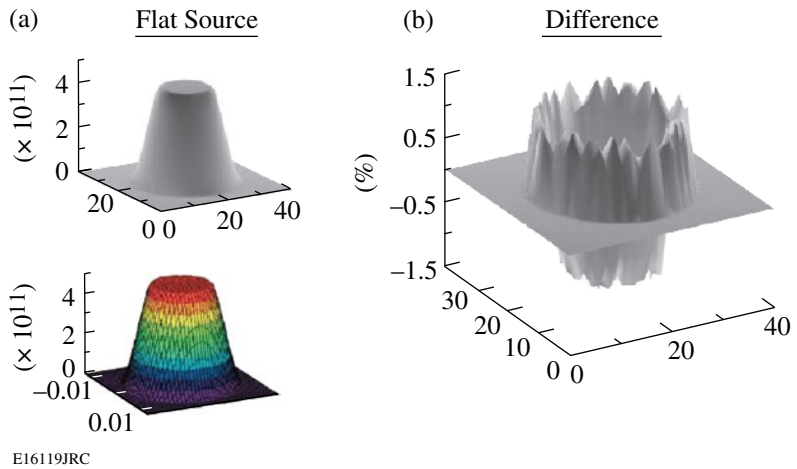

Figure 112.2
Comparison between the analytical solution and numerical simulations for a circular flat source. Graph (b) shows the relative difference between these two cases.

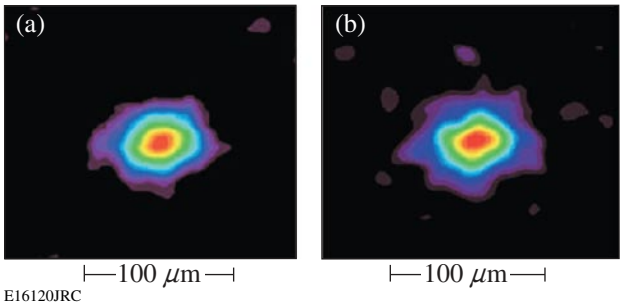

Figure 112.3
Image data (shot 35988, DT[10] CH[20], $Y_n = 8.5 \times 10^{12}$) deconvolved (a) with our code and (b) using filtered autocorrelation.[15]

Aperture Simulations

To test the sensitivity of the reconstructed images to aperture misalignment and fabrication errors, cases similar to the experimental setup described in Ref. 6 (and above) were simulated with the design code for a flat, circular source (Fig. 112.4). A biconic penumbral aperture with a central diameter of 2 mm and a pinhole with a central diameter of 10 μm were used to simulate a flat source 50 μm in diameter. In both cases, the FOV was 200 μm, the source–aperture distance was 26 cm, and the source–detector distance was 800 cm, with a magnification of 30.8. The aperture thickness was 10 cm. The maximum theoretical resolution of the simulated system for the deconvolved images was 4 μm [obtained from Eq. (2) with the assumption of a perfect alignment, and where k_c and δ_{rec} had a cumulative contribution of less than 0.1 μm]. Based on the discussion in **Reconstruction of the Detector-Plane Image** (p. 204), the tolerances for aperture fabrication and alignment can be set by the need to identify certain scale features in the reconstructed image. For this study, based on 50-μm cores on OMEGA, features of 10 μm were considered important. By incrementally moving the source relative to the system axis, an aperture misalignment was simulated. In a second phase, the aperture shape was elliptically distorted (with the eccentricity e defined in Fig. 112.4). In both cases, the error introduced in the deconvolved image was precisely defined.

1. Penumbral Apertures

The penumbral aperture's sensitivity to misalignment has been examined based on a set of simulations for apertures misaligned up to 2.36 mrad (corresponding to an offset of 250 μm relative to the primary axis). As the source is displaced, the reconstructed image appears more and more distorted (Fig. 112.5), i.e., the ratio between the horizontal and vertical dimensions increases. Image distortions within the range of the 10-μm feature limit were detectable for a misalignment angle as small as 0.4 mrad.

Aperture-fabrication defects were also analyzed for the penumbral aperture. Deviations from the circular conical shape were induced, and the coded image was transformed into an

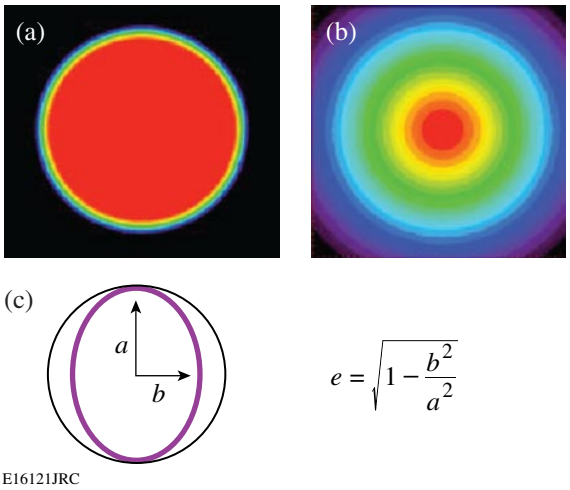

Figure 112.4
Examples of simulated raw images for a penumbral aperture (a) and a pinhole (b) seen at the detector plane level. (c) The aperture cross section and the distortion direction.

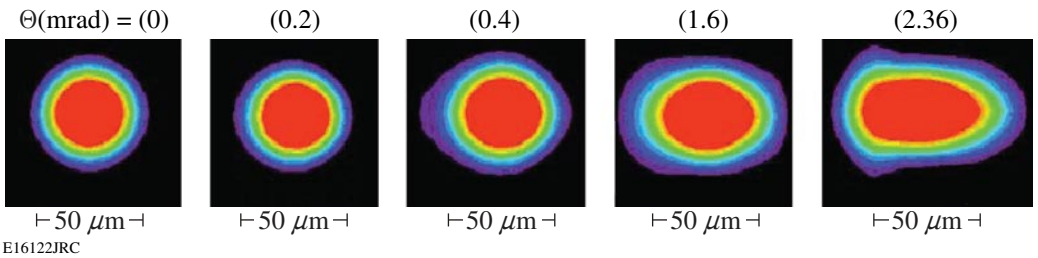

Figure 112.5
Reconstructed images of a penumbral aperture for various angles of misalignment (mrad) simulated by a source displacement.

ellipse. As the ellipse eccentricity (e) increased, the images became more and more distorted, as shown in Fig. 112.6. The subsequent modifications suggested that the aperture defects are as important as alignment for a penumbral imaging system (Fig. 112.6) and were detectable within the feature limit at an eccentricity of 0.15 or a 1.2% difference between the a and b axis parameters (this corresponds to a 24-μm out-of-round error for a 2-mm-diam aperture).

2. Pinhole Apertures

The pinhole sensitivity to misalignment has also been determined based on a set of simulations with progressively misaligned sources, in a geometry identical to the previous case. The same method has been used, first to verify the alignment tolerances (Fig. 112.7) and then to examine the influences of the fabrication defects (Fig. 112.8).

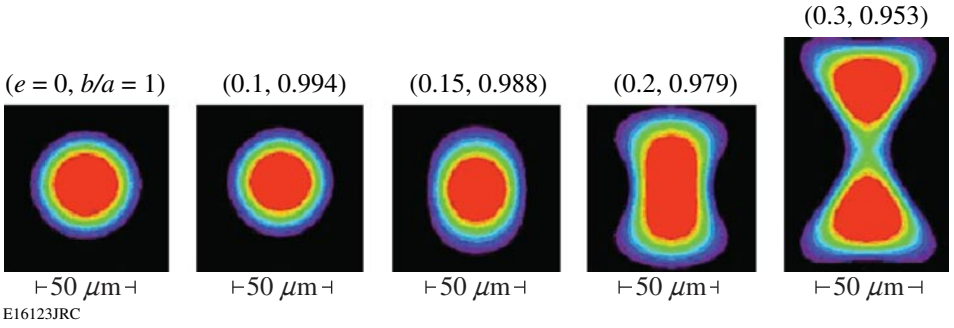

Figure 112.6
Reconstructed images of a penumbral aperture for various degrees of deformation.

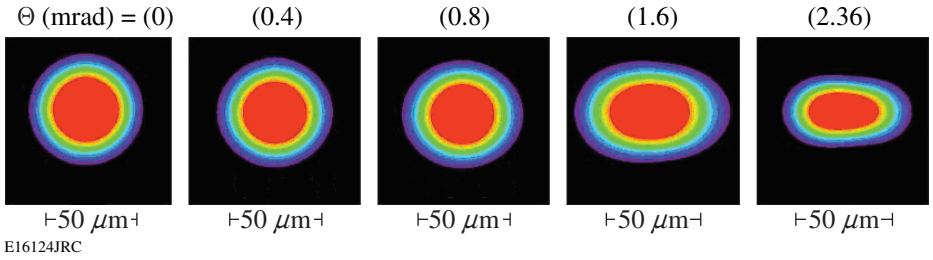

Figure 112.7
Reconstructed images of a pinhole for various angles of misalignment (mrad).

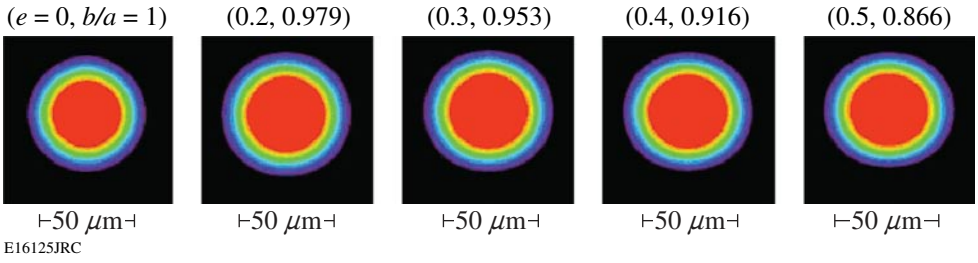

Figure 112.8
Reconstructed images of a pinhole for various degrees of deformation.

Aperture-fabrication defects were further analyzed for the pinhole. Deviations from the circular conical shape were induced and the coded image was transformed into an ellipse. As the ellipse eccentricity (e) increased, the images became more and more distorted, as shown in Fig. 112.8. Detectable distortions were observed at 0.8 mrad for the misalignment and for an eccentricity of 0.5 for the fabrication errors (a b/a ratio of 0.87 or an out-of-round tolerance of 1.4 μm for a 10-μm pinhole).

For both penumbral and pinhole apertures, the misalignment and fabrication errors can induce measurable false features in the deconvolution process. To minimize these features, alignment and fabrication tolerances can be determined from simulations such as those described above. For the imaging system previously described (and typical for a facility such as OMEGA), the requirements for a NI system designed to observe 10-μm features are summarized in Table 112.I. One can see that penumbral apertures are more sensitive to misalignment, while pinholes are more sensitive to fabrication errors.

Quantitative Analysis for the Errors Induced by Apertures

The distortions induced by the aperture-fabrication error or misalignment can be estimated by measuring the ratio between the reconstructed image axes for a flat disk neutron source. The values for angular misalignments and aperture deformations are detailed in Table 112.II.

The errors in the reconstructed image tend to increase approximately linearly with the alignment or deformation of the aperture (penumbral or pinhole).

Requirements for NI at the National Ignition Facility (NIF)

The NIF facility will use 192 laser beams for ICF with a total power of 1.8 MJ. A directly driven deuterium–tritium shell will have a diameter of 3 mm with a final compressed hot spot of about 80 μm. The geometric and energy constraints will not allow the NI imaging aperture to be placed closer than 50 cm from the source, implying, for a magnification similar to OMEGA, a much longer source–detector distance.

Simulations for penumbral and pinhole apertures similar to those used on OMEGA have been performed for the NIF case. The source–aperture distance was set to 52 cm and the source–detector distance was set to 16 m with a magnification value of M = 30.8, similar to the OMEGA simulation previously described. The FOV was maintained at the same value of 150 μm (with the apertures rescaled for the new geometry). The theoretical calculated resolution of the system was also 4 μm (calculated in the same way as for the OMEGA simulation from the previous section). The NIF requirements for a NI system can be summarized in Table 112.I.

Based on Table 112.I and the large source–aperture distance at the NIF, the limits obtained with the design tool suggest that penumbral apertures are slightly more sensitive to fabrication

Table 112.I: Tolerances for a NI system with a 10-μm resolution for the geometric configuration of OMEGA (upper) and the NIF (lower).

Penumbral Apertures (OMEGA)	Pinhole Apertures (OMEGA)
Misalignment of 0.4 mrad or source position off-center by 100 μm	Misalignment of 0.8 mrad or source position off-center by 200 μm
Fabrication eccentricity of 0.15 (i.e., 1.2% difference between the ellipse axes) or an absolute fabrication error of 24 μm	Fabrication eccentricity of 0.5 (i.e., ~14% difference between the ellipse axes) or an absolute fabrication error of 1.4 μm

Penumbral Apertures (NIF)	Pinhole Apertures (NIF)
Misalignment of 0.4 mrad	Misalignment of 0.4 mrad
Source position off-center by 200 μm	Source position off-center by 200 μm
Fabrication eccentricity of 0.15 (i.e., 1.1% difference between the ellipse axes) or an absolute fabrication error of 22 μm	Fabrication eccentricity of 0.4 (i.e., 8.3% difference between the ellipse axes) or an absolute fabrication error of 0.83 μm

Table 112.II: Angular misalignment versus axial deformation (upper). Deformation versus axial deformation (lower) of the reconstructed image for penumbral apertures and pinholes.

Angular Misalignment (mrad)	*b/a* (penumbral aperture)	Angular Misalignment (mrad)	*b/a* (pinhole)
0	1	0	1
0.2	1.007	0.2	1.045
0.4	1.195	0.4	1.13
1.6	1.375	1.6	1.53
2.36	1.785	2.36	1.79

Deformation (Eccentricity) for a Penumbral Aperture	*b/a* (penumbral)	Deformation (Eccentricity) for a Pinhole	*b/a* (pinhole)
1	1	1	1
1.006	1.025	1.021	1.055
1.012	1.2025	1.049	1.056
1.021	1.8875	1.092	1.098
1.049	5.428	1.154	1.16

errors (from 24 μm to 10 μm) with the angular sensitivity about the same, while pinholes become twice as sensitive to alignment (from 0.8 mrad to 0.4 mrad), with the same sensitivity to the relative fabrication error (1.4 μm).

Conclusions

A neutron-imaging (NI) design tool has been used to quantify the effects of aperture fabrication and alignment on reconstructed images. The simulations indicate that alignment tolerances of less than 1 mrad (current precision on OMEGA[8]) introduce measurable features in a reconstructed neutron image. Penumbral apertures are several times less sensitive to fabrication errors than pinhole apertures (as displayed in Tables 112.I and 112.II). A forthcoming publication will describe a NI bubble chamber that is being developed for high-resolution neutron imaging.

ACKNOWLEDGMENT

This work was supported by the U.S. Department of Energy Office of Inertial Confinement Fusion under Cooperative Agreement No. DE-FC52-92SF19460, the University of Rochester, and the New York State Energy Research and Development Authority. The support of DOE does not constitute an endorsement by DOE of the views expressed in this article.

REFERENCES

1. T. C. Sangster, R. L. McCrory, V. N. Goncharov, D. R. Harding, S. J. Loucks, P. W. McKenty, D. D. Meyerhofer, S. Skupsky, B. Yaakobi, B. J. MacGowan, L. J. Atherton, B. A. Hammel, J. D. Lindl, E. I. Moses, J. L. Porter, M. E. Cuneo, M. K. Matzen, C. W. Barnes, J. C. Fernandez, D. C. Wilson, J. D. Kilkenny, T. P. Bernat, A. Nikroo, B. G. Logan, S. Yu, R. D. Petrasso, J. D. Sethian and S. Obenschain, Nucl. Fusion **47** S686–S695 (2007).

2. J. D. Lindl, Phys. Plasmas **2**, 3933 (1995).

3. J. D. Kilkenny, M. D. Cable, C. A. Clower, B. A. Hammer, V. P. Karpenko, R. L. Kauffman, H. N. Kornblum, B. J. MacGowan, W. Olson, T. J. Orzechowski, D. W. Phillion, G. L. Tietbohl, J. E. Trebes, B. Chrien, B. Failor, A. Hauer, R. Hockaday, J. Oertel, R. Watt, C. Ruiz, G. Cooper, D. Hebron, L. Leeper, J. Porter, and J. Knauer, Rev. Sci. Instrum. **66**, 288 (1995).

4. R. J. Leeper, G. A. Chandler, G. W. Cooper, M. S. Derzon, D. L. Fehl, D. L. Hebron, A. R. Moats, D. D. Noack, J. L. Porter, L. E. Ruggles, J. A. Torres, M. D. Cable, P. M. Bell, C. A. Clower, B. A. Hammel, D. H. Kalantar, V. P. Karpenko, R. L. Kauffman, J. D. Kilkenny, F. D. Lee, R. A. Lerche, B. J. MacGowan, M. J. Moran, M. B. Nelson, W. Olson, T. J. Orzechowski, T. W. Phillips, D. Ress, G. L. Tietbohl, J. E. Trebes, R. J. Bartlett, R. Berggren, S. E. Caldwell, R. E. Chrien, B. H. Failor, J. C. Fernández, A. Hauer, G. Idzorek, R. G. Hockaday, T. J. Murphy, J. Oertel, R. Watt, M. Wilke, D. K. Bradley, J. Knauer, R. D. Petrasso, and C. K. Li, Rev. Sci. Instrum. **68**, 868 (1997).

5. T. J. Murphy, C. W. Barnes, R. R. Berggren, P. Bradley, S. E. Caldwell, R. E. Chrien, J. R. Faulkner, P. L. Gobby, N. M. Hoffman, J. L. Jimerson, K. A. Klare, C. L. Lee, J. M. Mack, G. L. Morgan, J. A. Oertel, F. J. Swenson, P. J. Walsh, R. B. Walton, R. G. Watt, M. D. Wilke, D. C. Wilson, C. S. Young, S. W. Haan, R. A. Lerche, M. J. Moran, T. W. Phillips, T. C. Sangster, R. J. Leeper, C. L. Ruiz, G. W. Cooper, L. Disdier, A. Rouyer, A. Fedotoff, V. Yu. Glebov, D. D. Meyerhofer, J. M. Soures, C. Stoeckl, J. A. Frenje, D. G. Hicks, C. K. Li, R. D. Petrasso, F. H. Séguin, K. Fletcher, S. Padalino, and R. K. Fisher, Rev. Sci. Instrum. **72**, 773 (2001).

6. D. Ress *et al*., Science **241**, 956 (1988).

7. T. R. Boehly, R. S. Craxton, T. H. Hinterman, J. H. Kelly, T. J. Kessler, S. A. Kumpan, S. A. Letzring, R. L. McCrory, S. F. B. Morse, W. Seka, S. Skupsky, J. M. Soures, and C. P. Verdon, Rev. Sci. Instrum. **66**, 508 (1995).

8. L. Disdier, A. Rouyer, I. Lantuéjoul, O. Landoas, J. L. Bourgade, T. C. Sangster, V. Yu. Glebov, and R. A. Lerche, Phys. Plasmas **13**, 056317 (2006).

9. R. K. Fisher, R. B. Stephens, L. Disdier, J. L. Bourgade, A. Rouyer, P. A. Jaanimagi, T. C. Sangster, R. A. Lerche, and N. Izumi, Phys. Plasmas **9**, 2182 (2002).

10. W. J. Hogan, E. I. Moses, B. E. Warner, M. S. Sorem, and J. M. Soures, Nucl. Fusion **41**, 567 (2001).

11. G. L. Morgan *et al*., Rev. Sci. Instrum. **72**, 865 (2001).

12. R. K. Fisher *et al*., Rev. Sci. Instrum. **72**, 796 (2001).

13. G. F. Knoll, *Radiation Detection and Measurement*, 3rd ed. (Wiley, New York, 2000).

14. L. Disdier, A. Rouyer, D. C. Wilson, A. Fedotoff, C. Stoeckl, J. L. Bourgade, V. Yu. Glebov, J.-P. Garçonnet, and W. Seka, Nucl. Instrum. Methods Phys. Res. A **489**, 496 (2002).

15. A. Rouyer, Rev. Sci. Instrum. **74**, 1234 (2003).